Chapter 5

Layout of Boussinesq couple-stress fluid flow over an exponentially stretching sheet with slip in porous space subject to variable magnetic field*

5.1 Introduction

The study of non-Newtonian fluids that does not obey the assumption of Newtonian fluids has received considerable attention in the last few years because of its pervasive applications in engineering and industry. The complex nature of non-Newtonian fluids has undoubtedly become an immense challenge to engineers, physicists and mathematicians. Several models have been proposed for the study of non-Newtonian fluids in the literature. It is also claimed that no single model exists which covers all properties of non-Newtonian fluids. These problems pose either challenging non-linearity in the governing equations, in addition to coupling or complex boundary conditions. In the presence of micron-sized suspended particles these problems endear themselves all the more to researchers who yearn for challenges. Depending upon the concentration and size of these suspended particles the available literature offers the following choice of

Published in **Multidiscipline Modeling in Materials and Stuctures, 16(5)(2020), pp.1131-1154.**

mathematical models for the suspensions in which (i) fluids with stress non-linearity proportional to the symmetric part of the velocity gradient (ii) fluids with internal angular momentum but the stress being linearly proportional to rate of strain. In this model, the almost invisible tiny-sized suspended particles which are in high concentration identify themselves with the carrier fluid almost to the point of camouflage. Most of these suspensions are naturally available and some technologically important ones are synthesized. This model is the Boussinesq-Stokes suspension model which is based on the couple stress theory of Stokes [280]. He has introduced that both polar and dipolar fluids are reduced to the theory of fluids with couple stresses. This model constrains the spin of the microelements to match with the vorticity of the carrier fluid. The consideration of couple stress in addition to classical Cauchy stress, has led to the development of several theories [281] of fluid microcontinua.

Boussinesq couple-stress fluids (or couple-stress fluids) have distinct features, such as the presence of couple stresses, body couples and non-symmetric stress tensor. In the category of non-Newtonian fluids, couple stress fluid has distinct features such as polar effects in addition to possessing large viscosity. The main feature of couple stresses is to introduce a size dependent effect. Classical continuum mechanics neglects the size effect of material particles within the continua. This is consistent with ignoring the rotational interaction among particles which results in symmetry of the force-stress tensor. The study of couple-stress fluids has vast industrial and technological applications such as the extrusion of polymer fluids, solidification of liquid crystals, wood coating, biocompatibility, bio-imging, biosensors etc. Many researchers have investigated couple-stress fluid models. Shantha et al. [282] have presented the free convective flow of a conducting couple stress fluid in a porous medium. Srinivasacharya and Kaladhar [283] have studied the mixed convection flow of couple stress fluid in a non-darcy porous medium considering Soret and Dufour effects. MHD flow and heat transfer of an exponential stretching sheet in a Boussinesq-Stokes suspension have been examined by Siddheshwar et al. [284]. Das et al. [285] have presented the slip flow of an optically thin radiating non-grey couple stress fluid past a stretching sheet.

The fluid flow over a stretching sheet is of crucial importance from both the theoretical and the practical view points because of its wide applications in the plastic engineering and metallurgy. Flows due to stretching sheet are significant in various engineering applications like paper production, aluminum bottle manufacturing processes, drawing of copper wires, metallurgical processes, spinning of fibers, production of rubber and plastic sheets, film coatings and crystal growing [286]. During the process of extrusion, the quality of the final product depends upon the rate of stretching

and the simultaneous heating or cooling during that process. So, fluid flow and heat transfer over the stretching sheet have a practical significance in many industrial processes. The rates of stretching and cooling have a significant influence on the quality of the final product with desired characteristics. The aforementioned processes involve cooling of a molten liquid by drawing into a cooling system. The properties desired for the product of such process mainly depend on two characteristics: the first is the cooling liquid used and the other is the rate of stretching. Liquids of non-Newtonian characteristics can be chosen as a cooling liquid as their flow and hence the rate of heat transfer can be regulated through some external means. Optimal rate of stretching is important, as rapid stretching results in sudden solidification, thereby destroying the properties expected from the product. Crane [148] has investigated the flow caused by the stretching of a sheet. Gupta and Gupta [287] have stressed that realistically stretching surface is not necessarily continuous. Most of the available literature deals with the study of boundary layer flow over a stretching surface where the velocity of the stretching surface is assumed linearly proportional to the distance from the fixed origin. However, it is often argued that realistically stretching of plastic sheet may not necessarily be linear. This situation is beautifully dealt by Kumaran and Ramanaiah [154] in their work on boundary layer fluid flow where probably first time, a general quadratic stretching sheet has been assumed. The various aspects of stretching problem have been investigated by many authors [288-295].

The study of magnetohydrodynamic flow of an electrically conducting fluid is of considerable interest in modern metallurgical and metal-working processes. The process of fusing of metals in an electrical furnace by applying a magnetic field and the process of cooling of the wall inside a nuclear reactor containment vessel are good examples of such fields [296]. Some important applications of MHD radiative heat transfer include space technology, hypersonic flights, power generation systems, furnace design, design of rocket ignition chambers, design of high temperature gas cooled nuclear/atomic reactors, medical industry and so on. Many processes in engineering areas occur at high temperature and knowledge of radiative heat transfer becomes very important for the design of pertinent equipment [297]. In controlling momentum and heat transfers in the boundary layer flow of different fluids over a stretching sheet, applied magnetic field may play an important role [298]. Kumaran et al. [164] have investigated that magnetic field makes the streamlines steeper which results in the velocity boundary layer being thinner. The heat transfer analysis of boundary layer flow with radiation is also important in electrical power generation, astrophysical flows, solar power technology, space vehicle re-entry, design of pertinent equipment and other industrial areas. Raptis

et al. [118] have reported the effect of thermal radiation on the MHD flow of a viscous fluid past a semi-infinite stationary plate.

In recent years, MHD boundary layer flow through porous medium has gained attention of many researchers because in electrically conducting fluid, applied magnetic field influences heat generation/absorption and in result controls the desired characteristics of final product. Several researchers have considered the stretching sheet problems embedded in porous medium under the influence of magnetic field for various types of non-Newtonian fluids. Cortell [299] has analyzed MHD flow of second grade fluid flow over stretching sheet embedded in porous medium with chemical reaction. The two dimensional boundary layers flow through porous medium over vertical stretching sheet under the influence of magnetic field has been discussed by Hayat et al. [300]. The steady state electrically conducting flow of Casson fluid over a stretching sheet in a porous medium has been reported by Shawky [301]. Nadeem et al. [302] have explored three dimensional electrically conducting boundary layer flow of Casson fluid over stretching sheet saturated in a porous medium. Jat et al. [303] have analyzed MHD boundary layer flow of viscous fluid past nonlinearly stretching sheet embedded in porous medium. They have observed that velocity decreases with increasing porosity parameter which results in increasing the magnitude of skin friction coefficient.

On the other hand, slip condition has significant applications in various industries and is very efficient in manufacturing process. It is a common belief that heat transfer can be increased by adding velocity slip at the boundary. The abundant literature on the boundary layer flow over a stretching sheet is limited to non-Newtonian fluids with traditional no-slip flow boundary condition over various stretching geometry such as linear and non-linear stretching sheet and a little attention is given to stretching sheet with slip boundary condition. However, fluids with micro-scale or nano-scale dimensions have flow behavior that greatly differs from the traditional fluid flow characteristics and belongs to the slip flow regime. For the flow in the slip regime, the fluid motion still obeys the Navier-Stoke's equations, but with slip velocity, temperature and concentration boundary conditions. For instance, the flow in many applications of micro/nano systems such as hard disk drive, micro-pump, micro-valve and micro-nozzles is in slip transition regime, which is characterized by slip boundary at the wall. Beavers and Joseph [304] are the first who have used partial slip to the fluid past permeable wall. The addition of velocity slip at the wall also plays a vital role for flow in micro devices [305]. For this reason, researchers have paid considerable attention to include the slip condition at wall rather than no slip condition. The slip flow of elastico-viscous fluid induced by a stretching sheet has been reported by Ariel et al. [306]. Wang

[157, 307] has analyzed the viscous flow due to a stretching sheet with surface slip and suction. Fang et al. [163, 308] have obtained the exact solution of an MHD slip flow over a stretching sheet. The second order slip flow and heat transfer over a stretching sheet with non-linear Navier boundary condition have been investigated numerically by Nandeppanavar et al. [309]. Zhu et al. [310] have presented the second-order slip MHD flow and heat transfer of nanofluids with thermal radiation and chemical reaction. Ullah et al. [311] have inspected the effect of slip condition on MHD free convective flow of non-Newtonian fluid over a nonlinearly stretching sheet saturated in porous medium with Newtonian heating. They have observed that slip effect is more pronounced on temperature profile in comparison with velocity profile. Several authors have broadened the notion of slip regime for various fluid models [312-314].

Numerous number of research papers on a stretching sheet have been published by considering various governing parameters such as suction/injection, porosity, magnetic field, permeability of porous media and thermal radiation with different types of fluids such as Newtonian, non-Newtonian, polar and couple stress fluids. The various aspects of momentum and heat transfer characteristics in boundary layer flow over a stretching surface have been considered by many authors [315-324]. Time dependent electrically conducting mixed convection flow over an exponentially stretching sheet with heat absorption/generation has been analyzed by Elbashbeshy et al. [325]. Singh and Makinde [326] have studied an MHD slip flow of viscous fluid over an isothermal reactive stretching sheet. Seini and Makinde [327] have presented an MHD boundary layer flow due to exponential stretching surface with radiation and chemical reaction. Hayat et al. [328] have presented the stagnation-point flow of couple stress fluid with melting heat transfer. MHD boundary layer flow and heat transfer towards an exponentially stretching sheet embedded in a thermally stratified medium subject to suction have been presented by Mukhopadhyay [329]. Turkyilmazoglu [330] has obtained an exact solutions for two-dimensional laminar flow over a continuously stretching or shrinking sheet in an electrically conducting quiescent couple stress fluid.

Sheikholeslami et al. [331] have discussed the forced convective heat transfer with variable magnetic field using two phase model. The effect of non-uniform magnetic field on forced convection heat transfer of Fe_3O_4- water nanofluid has examined by Sheikholeslami et al. [332]. Kandelousi [333] has inspected the effect of spatially variable magnetic field on ferrofluid flow and heat transfer considering constant heat flux boundary condition. Ahmad and Ishak [334] have studied the MHD flow and heat transfer of a Jeffrey fluid over a stretching sheet with viscous dissipation. Sandeep et al. [335] have analyzed the unsteady magnetohydrodynamic radiative flow and heat

transfer characteristics of a dusty nanofluid over an exponentially permeable stretching surface in presence of volume fraction of dust and nano particles. Ferdows et al. [336] have discussed the influence of viscous dissipation and Hall current on the boundary layer flow over a stretching surface. Mabood et al. [337] have reported the MHD boundary layer flow of a viscous incompressible fluid over an exponentially stretching sheet. Homotopy analysis method (HAM) has been used to get accurate and complete analytic solution. They have found that the magnetic and radiation parameters have major effects on the flow field, skin friction coefficient and rate of heat transfer. Shahzad et al. [338] have presented the magnetohydrodynamics boundary layer flow and heat transfer of the Jeffrey nanofluid over a stretching sheet in the presence of viscous dissipation and Joule heating. The magnetohydrodynamic mixed convection flow of a Carreau nanofluid with heat and mass transfer towards an exponentially stretching sheet with the effects of partial slip, convective boundary condition, Soret and Dufour has been discussed by Sharada and Shankar [339].

From the above discussion, it is very much clear that slip effects on the MHD flow and heat transfer of Boussinesq couple-stress fluid over an exponentially stretching sheet embedded in porous medium has not yet been reported. The main focus of the present chapter is to address the slip flow and heat transfer of Boussinesq couple-stress fluid over an exponentially stretching sheet embedded in a porous medium in the presence of variable transverse magnetic field and thermal radiation with viscous and Joule heating. Suitable similarity transformations are deployed to the governing partial differential equations for conversion to the ordinary differential equations which are solved numerically. Employing Runge-Kutta method coupled with shooting technique, numerical computations up to desired level of accuracy have been performed for different values of pertinent flow parameters. The velocity and temperature profiles for pertinent parameters are plotted graphically with the help of bvp4c MATLAB subroutine followed by Shampine et al. [340]. Due to the physical significance of the shear stress and rate of heat transfer, their numerical results are presented and also analyzed. The analysis of the results obtained shows that the flow field is influenced noticeably by the slip parameter in the presence of applied transverse magnetic filed, thermal radiation, viscous and Joule heating. The present study will not only provide useful information for applications, but also serve as a complement to the previous studies.

5.2 Mathematical model

Consider steady MHD slip flow of a viscous incompressible electrically conducting Boussinesq couple-stress fluid over an exponentially stretching sheet coinciding with the plane $y = 0$. The flow is confined to $y > 0$. The x-axis is taken along the stretching sheet toward the direction of motion of the flow and the y-axis is normal to the sheet surface(see Fig.5.1). The sheet is stretched along the x-axis in its own plane with the velocity $U_w(x)$ which is a exponential function of the distance from the origin. The flow is produced due to the exponentially stretch of the sheet away from the leading edge. The sheet surface is heated to a variable temperature $T_w(x)$ while the temperature of uniform ambient quiescent fluid is T_∞. It is assumed that the surface temperature is higher than the ambient temperature, i.e. $T_w > T_\infty$. A variable magnetic field $B(x)$ is applied along the y-axis which generates magnetic effects in the y-direction. The impact of the induced magnetic field is neglected. This can be justified for MHD flow for sufficiently small magnetic Reynolds number. It is also assumed that the external electric field is zero and the electric field due to the polarization of charges is negligible. The sheet is placed in a porous medium with permeability K^*. The porous medium is considered as homogeneous as well as isotropic is in local thermal equilibrium with the fluid.

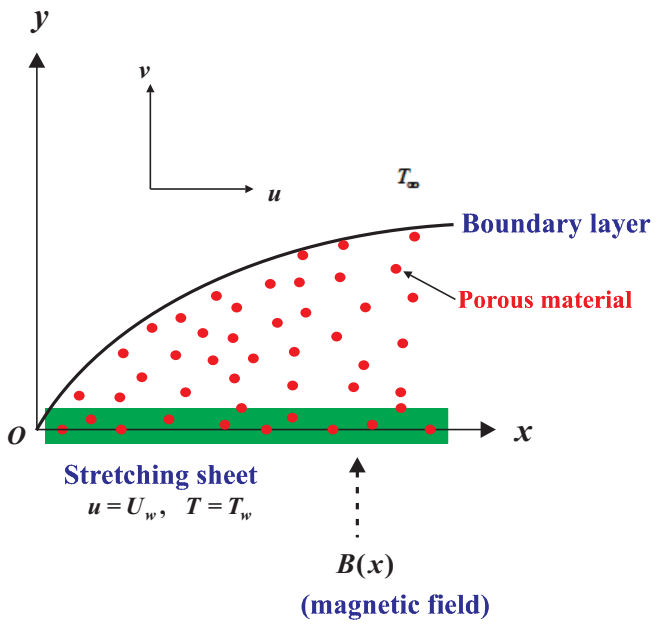

Fig.5.1: *Sketch of physical problem and coordinate system*

In the light of above assumptions and based on the usual boundary layer approximations and Darcy's model of flow in porous medium, the MHD flow and heat transfer of a radiated couple-stress fluid through a porous medium are governed by the following equations [284, 285]:

$$\frac{\partial u}{\partial x} + \frac{\partial u}{\partial y} = 0, \tag{5.1}$$

$$u\frac{\partial u}{\partial x} + v\frac{\partial u}{\partial y} = \nu\frac{\partial^2 u}{\partial y^2} - \nu^*\frac{\partial^4 u}{\partial y^4} - \frac{\sigma B_0^2}{\rho}\,u - \frac{\nu}{K^*}\,u, \tag{5.2}$$

$$u\frac{\partial T}{\partial x} + v\frac{\partial T}{\partial y} = \frac{k}{\rho\, c_p}\frac{\partial^2 T}{\partial y^2} - \frac{1}{\rho\, c_p}\frac{\partial q_r}{\partial y} + \frac{\mu}{\rho\, c_p}\left(\frac{\partial u}{\partial y}\right)^2 + \frac{\sigma}{\rho\, c_p}B_0^2 u^2, \tag{5.3}$$

where u and v are the velocity components of couple-stress fluid along the x- and y-directions, respectively, T the temperature of the couple-stress fluid, ρ the couple-stress fluid density, μ the dynamic viscosity of the couple-stress fluid, ν the kinematic viscosity, ν^* the couple stress viscosity, K^* the permeability of porous medium for the couple-stress fluid, k the thermal conductivity, c_p the specific heat at constant pressure and q_r the radiative heat flux.

The implemented boundary conditions for the problem are given by [284, 285]

$$\begin{aligned} &u = U_w + L^*\left(\frac{\partial u}{\partial y}\right),\ \ v = 0,\ \ \frac{\partial^2 u}{\partial y^2} = 0,\ \ T = T_w = T_\infty + T_0 e^{\frac{x}{L}}\ \text{ at }\ y = 0,\\ &u \to 0,\ \ \frac{\partial^2 u}{\partial y^2} \to 0,\ \ T \to T_\infty\ \text{ as }\ y \to \infty, \end{aligned} \tag{5.4}$$

where $U_w = U_0 e^{\frac{x}{L}}$, U_0 is the reference velocity, T_0 the reference temperature, L the reference length and $L^* = L\, e^{-\frac{x}{2L}}$ the velocity slip factor. When $L^* = 0$, the no-slip condition is recovered.

The effect of radiation is manifested in the form of enhanced thermal diffusivity. The radiative heat flux component on the surface is expressed with the help of Stefan-Boltzman law. The Rosseland approximation [341] permits the simplification of the governing integro-differential equation for radiative energy balance into a Fourier-type diffusion equation analogous to that describing heat conduction, potential flow or electro static potential(Coulomb's law) which is valid for optically thick media in which radiation only propagates a limited distance prior to experiencing scattering or absorption (Mehmood et al. [342]). The energy transfer depends only on the conditions in the area near the position under consideration. Thus, the radiative heat flux term is simplified by using the Rosseland approximation for an optically thick fluid according to

$$q_r = -\frac{4\sigma^*}{3k^*}\frac{\partial T^4}{\partial y}, \tag{5.5}$$

where σ^* is the Stefan-Boltzman constant and k^* the Rosseland mean absorption coefficient. This approximation is valid at points optically far from the bounding surface and good only for intensive absorption which is for an optically thick boundary layer [185, 343, 344]. It is assumed that the temperature difference within the flow is sufficiently small such that the term T^4 may be expressed as a linear function of temperature. This is done by expanding T^4 in a Taylor series about the free stream temperature T_∞ as follows:

$$T^4 = T_\infty^4 + 4T_\infty^3(T - T_\infty) + 6T_\infty^2(T - T_\infty)^2 + \cdots \tag{5.6}$$

Neglecting higher-order terms in (5.6) beyond the first order in $(T - T_\infty)$, result in

$$T^4 = 4T_\infty^3 T - 3T_\infty^4. \tag{5.7}$$

On the use of (5.5) and (5.7), equation (5.3) reduces to

$$u\frac{\partial T}{\partial x} + v\frac{\partial T}{\partial y} = \frac{k}{\rho\, c_p}\frac{\partial^2 T}{\partial y^2} + \frac{16\sigma^* T_\infty^3}{3k^*\rho c_p}\frac{\partial^2 T}{\partial y^2} + \frac{\mu}{\rho\, c_p}\left(\frac{\partial u}{\partial y}\right)^2 + \frac{\sigma}{\rho\, c_p}B_0^2 u^2. \tag{5.8}$$

To obtain similarity solutions, it is assumed that the variable magnetic field $B(x)$ is of the form:

$$B(x) = B_0 e^{\frac{x}{2L}}, \tag{5.9}$$

where B_0 is the constant magnetic field.

The continuity equation (5.1) is satisfied by introducing a stream function $\psi(x, y)$ defined in the usual form as

$$u = \frac{\partial \psi}{\partial y}, \quad v = -\frac{\partial \psi}{\partial x}. \tag{5.10}$$

The following similarity variables are introduced to transform the momentum and energy equations to ordinary differential equations using similarity variables [327]:

$$\begin{aligned} &x^* = \frac{x}{L}, \quad y^* = \frac{y}{L}, \quad \eta = y^*\left(\frac{Re}{2}\right)^{\frac{1}{2}} e^{\frac{x^*}{2}}, \\ &\psi^*(x^*, y^*) = \frac{\psi(x, y)}{\nu} = (2Re)^{\frac{1}{2}}\, f(\eta)\, e^{\frac{x^*}{2}}, \quad \theta = \frac{T - T_\infty}{T_0\, e^{\frac{x^*}{2}}}, \end{aligned} \tag{5.11}$$

where η is the dimensionless similarity variable, $f(\eta)$ the dimensionless stream function and $\theta(\eta)$ the dimensionless temperature.

Substituting the equation (5.11) into equations (5.2) and (5.8), we obtain the following ordinary differential equations

$$CRe\, f^V - 2f''' - 2f\, f'' + 4f'^2 + 4\left(M^2 + \frac{1}{Da}\right) f' = 0, \tag{5.12}$$

$$\left(1 + \frac{4}{3}N\right)\theta'' - Pr(\theta f' - f\theta') + Pr\, Ec(f''^2 + 2M^2 f'^2) = 0, \tag{5.13}$$

where $M^2 = \frac{\sigma\, B^2\, L}{\rho\, U_w}$ is the magnetic parameter, $C = \frac{\nu^* e^{x^*}}{\nu\, L^2}$ the couple stress parameter, $Re = \frac{U_0\, L}{\nu}$ the Reynolds number that represents the ratio of the inertial force to the viscous force, $Da = \frac{ReK^* e^{x^*}}{L^2}$ the Darcy number which signifies the relative permeability of the porous regime (high Da implies high permeability and vice versa), $N = \frac{4\sigma^* T_\infty^3}{k^* k}$ is the radiation parameter, $Ec = \frac{U_w^2}{c_p(T_w - T_\infty)}$ the Eckert number which defines the ratio of the kinetic energy of the flow to the enthalpy difference i.e. the degree of mechanical energy dissipated as heat via internal friction and $Pr = \frac{\rho\, \nu\, c_p}{k}$ the Prandtl number which measures the ratio of momentum diffusivity to the thermal diffusivity.

The transformed boundary conditions take the following form

$$\begin{aligned} &f(0) = 0, \;\; f'(0) = 1 + \lambda\, f''(0), \;\; f'''(0) = 0, \;\; \theta(0) = 1, \\ &f'(\infty) \to 0, \;\; f'''(\infty) \to 0, \;\; \theta(\infty) \to 0, \end{aligned} \tag{5.14}$$

where primes denote derivatives with respect to η, $\lambda = \left(\frac{Re}{2}\right)^{\frac{1}{2}} e^{\frac{x^*}{2}}$ is the velocity slip parameter. The no-slip case is recovered for $\lambda = 0$.

5.3 Numerical method for solution

Most of the boundary layer problems are described by a set of nonlinear partial differential equations. However, due to the strongly nonlinear and unconventional nature of boundary layer problems, the solving processes are extremely intricate, and the analytical solutions are hardly obtained. In recent past, various numerical methods have been deployed to solve those problems. The mathematical model of non-dimensional ordinary differential equations (5.12) and (5.13) subject to the boundary conditions (5.14) are attempted to solve the present problem numerically. The highly nonlinear momentum and energy equations are transform into similarity equations and then solved numerically by employing the fourth order Runge-Kutta integration scheme with shooting technique [345]. Runge-Kutta method is the fourth order method meaning that the local truncation error is of order $O(\Delta\eta)^5$ whereas the total accumulated error is of order $O(\Delta\eta)^4$. This is a usual case that, the truncation error also includes discretization error, which is the error that arises from taking the finite number of steps in the

computation to approximate an infinite process. The resulting higher order ordinary differential equations are reduced to first order differential equations by letting

$$x_1 = f,\ \ x_2 = f',\ \ x_3 = f'',\ \ x_4 = f''',\ \ x_5 = f^{(IV)},\ \ x_6 = \theta,\ \ x_7 = \theta'. \tag{5.15}$$

Thus, the corresponding coupled higher order non-linear differential equations (5.12) and (5.13) become

$$\begin{aligned}
x_1' &= x_2,\\
x_2' &= x_3,\\
x_3' &= x_4,\\
x_4' &= x_5,\\
x_5' &= \frac{2}{CRe}[x_4 + x_1x_3 - 2x_2^2 - 2M^2x_2 - \frac{2}{Da}x_2],\\
x_6' &= x_7,\\
x_7' &= \left[Pr(x_2x_6 - x_1x_7) - Pr\,Ec\left(x_3^2 + 2M^2x_2^2\right)\right] / \left(1 + \frac{4}{3}N\right)
\end{aligned} \tag{5.16}$$

with the boundary conditions:

$$\begin{aligned}
&x_1(0) = 0,\ x_2(0) = 1 + \lambda\, x_3(0),\ x_3(0) = s_1,\ x_4(0) = 0,\\
&x_5(0) = s_2,\ x_6(0) = 1,\ x_7(0) = s_3,
\end{aligned} \tag{5.17}$$

where s_1, s_2 and s_3 are unknown which are to be determined as a part of the numerical solution technique.

In the shooting technique, convenient values of the unspecified initial conditions s_1, s_2 and s_3 in (5.17) are guessed and equation (5.16) integrated numerically by taking the help of the standard fourth-order Runge-Kutta formula and a shooting technique as an initial valued problem to a given terminal point with the successive iteration step length 0.01. The accuracy of the assumed missing initial condition is checked by comparing the calculated value of the dependent variable at the terminal point with its given value there. If there any difference exists, improved values of the missing initial conditions must be obtained and the process is continued until the boundary conditions are approximately satisfied for $\eta \to \infty$. The numerical computations are done by a written program which uses a symbolic and computational computer language (MatLab bvp4c routine). The step-size is chosen as $\Delta\eta = 0.01$. The process is repeated until we get the results with error less than the specified degree of accuracy 10^{-6}. For the constant step size (or mesh size) $\Delta\eta$ depending on flow parameters, the convergence criteria of the fourth order Rung-Kutta integration scheme are satisfied successfully.

In order to verify the reliability and accuracy of the applied numerical scheme, a comparison of the present results with the available published results of Seini and Makinde [327] corresponding to the values of shear stress $[-f''(0)]$ in the absence of couple stress fluid, hydrodynamic slip and porous medium is made and presented in Table 5.1. The results are found in excellent agreement.

Table 5.1: *Shear stress $-f''(0)$ for different values of M^2 when $C = 0$, $\lambda = 0$ and $Da = \infty$ compared to previous results*

M^2	Seini and Makinde [327]	Present study
2	1.912624	1.9126223
5	2.581130	2.5811330
10	3.415280	3.4152962

5.4 Results and discussion

The theory of couple stress fluids due to Stokes is used to model an MHD slip flow of couple-stress fluid over an exponentially stretching sheet embedded in a porous medium Runge-Kutta integration technique is applied for numerical solution. In order to get a physical insight of the problem, numerical computation has been carried out using the method described in the previous section for various values of the pertinent parameters, viz. magnetic parameter M^2, couple stress parameter C, Darcy number Da, slip parameter λ, radiation parameter N, Prandtl number Pr and Eckert number Ec on the fluid velocity and temperature profiles, shear stress and rate of heat transfer. The parameters are chosen arbitrarily where $Pr = 0.71$ corresponds physically to air at 20^oC, $Pr = 1$ corresponds to electrolyte solution such as salt water and $Pr = 7$ corresponds to water. As $C \to \infty$, the couple stress fluid reduces to Newtonian fluid. $Da = \infty$ corresponds to non-porous medium and $Da \neq \infty$ corresponds to porous medium. Also $Ec = 0$ presents the absence of viscous and Joule dissipation heating. For a large value of slip parameter λ which corresponds to a very small x at the leading edge, the boundary layer assumption is not appropriate, i.e. the boundary layer equations become inaccurate. Further, the Knudsen number is greater than 0.1 for a large λ and hence the Navier-Stokes equation be unsuccessful to model the flow regime. We therefore bound the discussion in this chapter to a relatively small range of λ from 0 to 1 as this reveals the slip flow region. The default values of the other parameters are mentioned in the description of the respective figures.

5.4.1 Effects of parameters on velocity profiles

The velocity profiles are considerably decreased for increasing values of magnetic parameter M^2 shown in Fig.5.2(a). This is predictable, since the application of applied

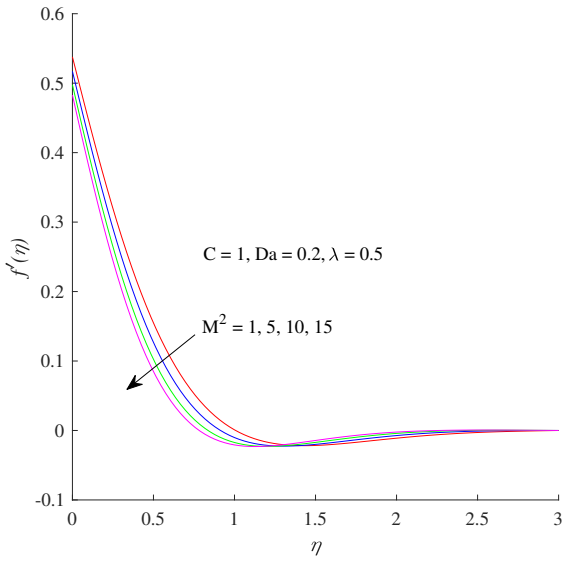

Fig.5.2(a): *Velocity profiles varying* M^2

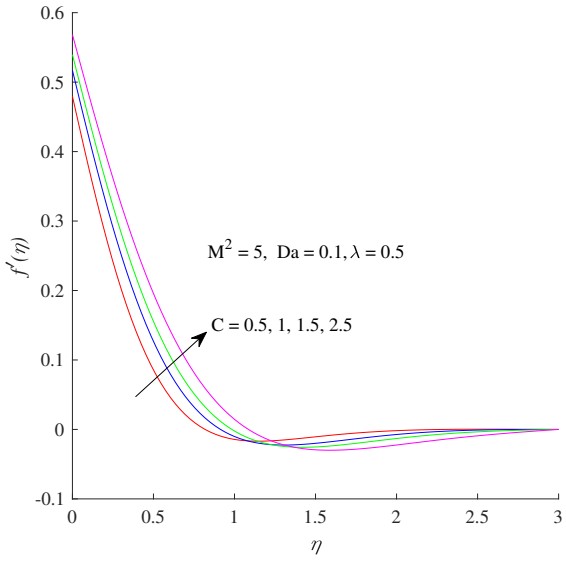

Fig.5.2(b): *Velocity profiles varying* C

transverse magnetic field in an electrically conducting fluid gives rise to Lorentz force which tends to resist the fluid flow. Fig.5.2(b) reveals that the velocity profiles are

found to boost near the sheet surface and reduces away from the surface of the sheet for elevation of couple-stress parameter C. Increasing values of C results an increase in thickness of the the momentum boundary layer. Hence, the flow can be controlled by choosing a suitable value of couple-stress parameter. The effect of Darcy number Da

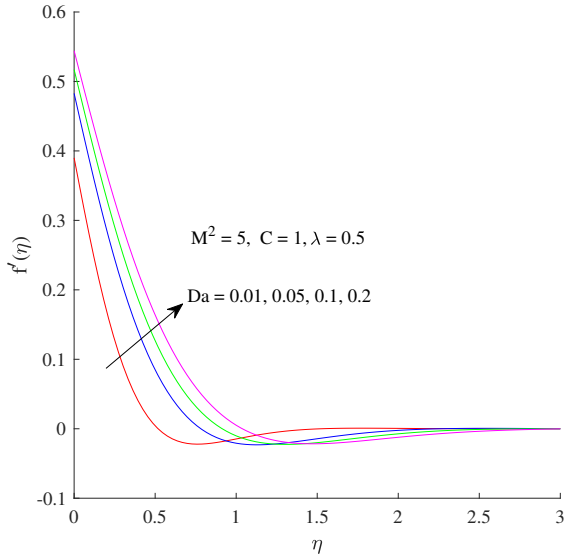

Fig.5.2(c): *Velocity profiles varying Da*

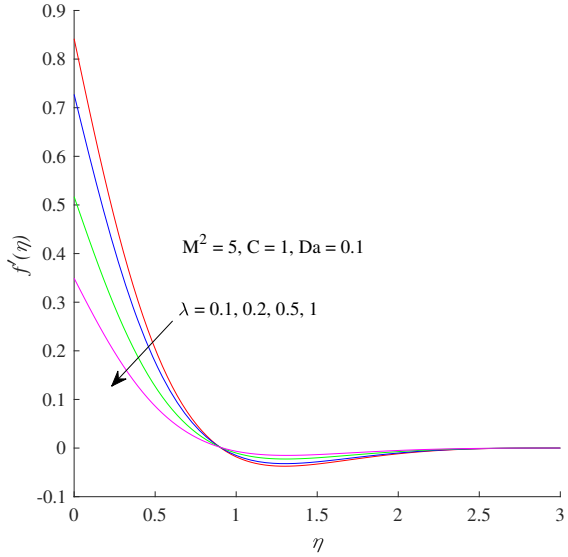

Fig.5.2(d): *Velocity profiles varying* λ

on velocity profile and its associated boundary layer thickness is demonstrated in Fig.5.2(c). As Darcy number Da grows, the velocity profile also increases near the

sheet surface and a reverse trend is observed away from the sheet. Practically, Darcy number measures the permeability of the porous medium. The permeability is defined as the surface area that is open to flow. For large values of Darcy number, fluid gets more space to flow and provides less resistance to the fluid flow, due to which the fluid velocity enhances. Fig.5.2(d) is presented to analyze the impact of slip parameter λ on the velocity profile. The velocity profile is a decreasing function of λ. Physically, when slip occurs, the slipping fluid shows a reduction in the surface skin-friction between the fluid and the stretching sheet because not all the pulling force of the stretching sheet can be transmitted to the fluid. So, increasing in λ causes diminishing behaviour in velocity profile in the region of the boundary layer.

5.4.2 Effects of parameters on temperature profiles

Fig.5.3 is drawn to expose the impact of flow parameter on the non-dimensional temperature profile and the associated boundary layer thickness. In Fig.5.3(a), the impact of increasing magnetic parameter on temperature profile is portrayed. The temperature

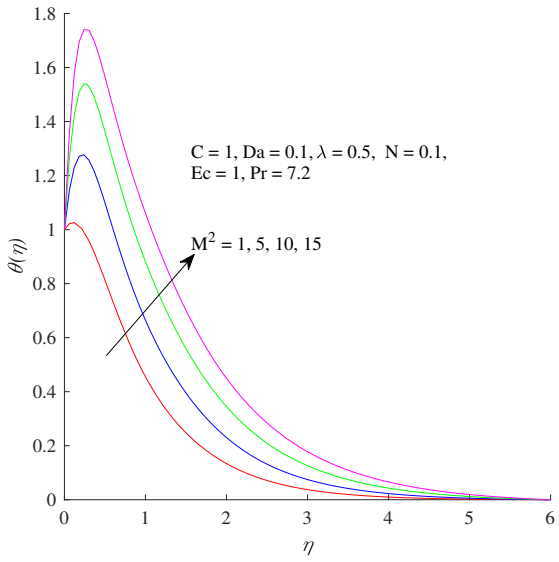

Fig.5.3(a): *Temperature distributions varying* M^2

profile and the thermal boundary layer thickness show noticeable increasing behaviour for higher values of magnetic parameter M^2. This is quite consistent with the physical situation as the application of magnetic field initiates Lorentz force which generates Ohmic heat and also additional skin frictional heating, due to stress work that results in higher temperature near the sheet with the growing thermal boundary layer thick-

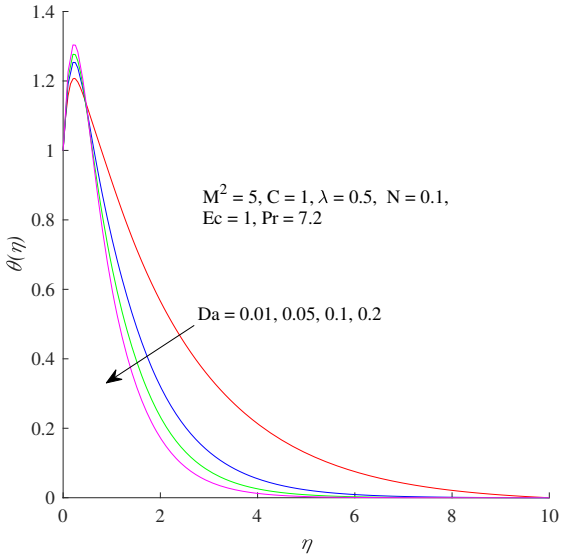

Fig.5.3(b): *Temperature distributions varying Da*

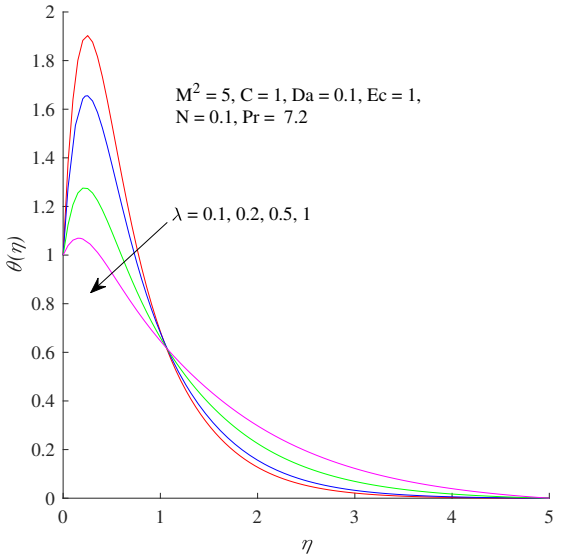

Fig.5.3(c): *Temperature distributions varying λ*

ness. Fig.5.3(b) shows the effect of Darcy number *Da* on the temperature profiles. The temperature profile increase due to the growth of Darcy number in the vicinity of the sheet surface as a result of velocity increase which increases the viscous dissipation. When fluid flows through a porous medium, internal energy is dissipated in form of heat due to friction between fluid and the porous medium. Such internal energy is not so small when the porous medium possesses larger permeability. Hence, the increase in

temperature profiles are physically justified. It can also be observed that temperature increases more rapidly in porous medium as compared to low intensity porous medium.

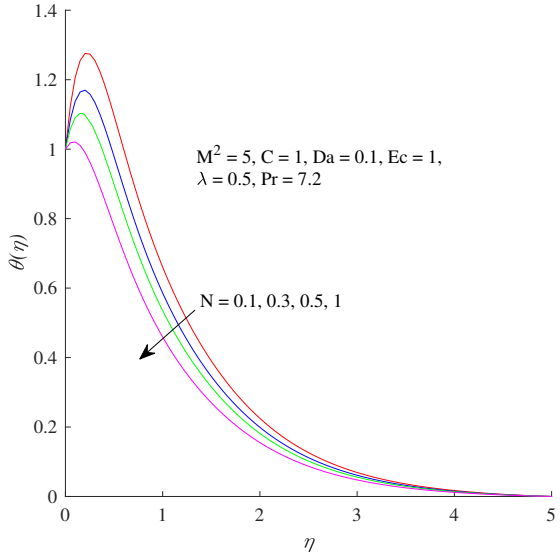

Fig.5.3(d): *Temperature distributions varying N*

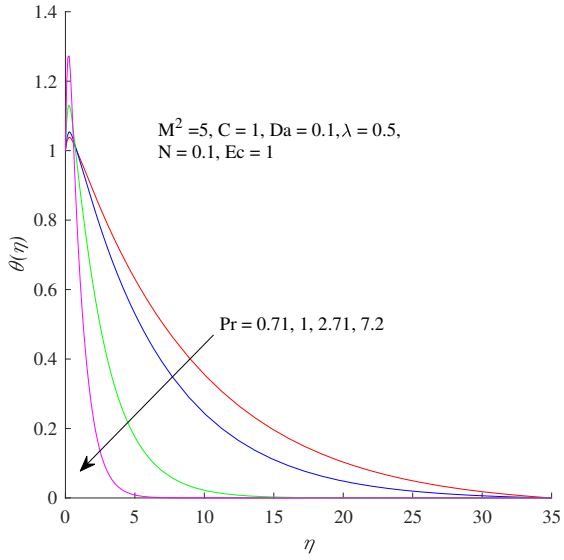

Fig.5.3(e): *Temperature distributions varying Pr*

The effect of slip parameter λ on the temperature profiles is displayed in Fig.5.3(c). It is noticed that the temperature profile decreases near the sheet surface ($\eta \leq 1.1$) and increase away from the sheet ($\eta > 1.1$) when λ is increased. This is coherent because an increase in slip parameter leads to decline internal heat energy generation results

in a decrease of heat transfer close to the sheet surface. An increase in thermal radiation N causes to decrease in the temperature profiles within the boundary layer and the thermal boundary layer thickness is therefore also decreased as shown in Fig.5.3(d).

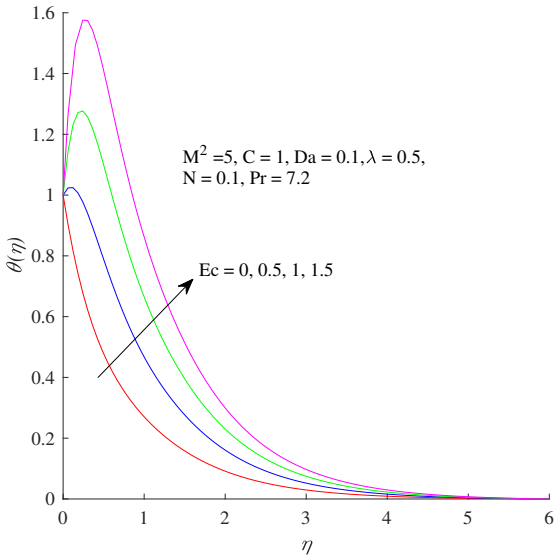

Fig.5.3(f): *Temperature distributions varying Ec*

The increase of radiation parameter implies the release of heat energy from the flow region by means of thermal radiation; this can also be enlighten by the fact that the effect of thermal radiation is to enhance the rate of energy transport to the fluid and as a result decrease the fluid temperature. Fig.5.3(e) highlights the effects of Prandtl number Pr on temperature profiles. An increase in Prandtl number Pr results a decrease in temperature profiles. The reason is that smaller values of Prandtl number are correspondent to incresing thermal conductivity and therefore heat is capable of diffusing away from the heated surface more rapidly than at higher values of Pr. Thus the fluid temperature reduces more rapidly for water than for air and electrolyte solution. An increase in Prandtl number conveys a decline in the thermal boundary layer thickness. Fig.5.3(f) illustrates the influence of Eckert number Ec on temperature profiles in the boundary layer. The fluid temperature is seen to increase with Ec. Eckert number signifies the ratio of the kinetic energy of the flow to the boundary layer enthalpy differences. It represents the conversion of the kinetic energy into internal energy by work done against the viscous fluid stresses. The positive Eckert number means cooling of the surface of the stretching sheet, i.e. loss of heat from the surface of the stretching sheet to the fluid. Hence, greater viscous dissipative heat causes a rise in the fluid tem-

perature. It can also be observed that the thermal boundary layer thickness becomes thicker for increased Eckert number. Furthermore, it is revealed that there would be a higher temperature for the situation when $Ec = 1$ than for the case when $Ec = 0$. This is due to the fact that energy is stored in the fluid region as a result of dissipation owing to viscosity and elastic deformation. The temperature profiles are maximum in the vicinity of the surface of the stretching sheet. Temperature profiles all decay from it maximum value at the sheet to zero in the free stream, that is, converge at the outer edge of the boundary layer.

5.4.3 Effects of parameters on stream function

Fig.5.4 presents the stream function for several values of M^2, Da, C and λ. In Figs.5.4(a)-5.4(b), it is found that stream lines very slightly distort in the presence of magnetic filed ($M^2 = 10$). Effect of stream lines can be observed in the presence of porous medium in Figs.5.4(c)-5.4(d). It is seen that stream lines distort and are low intensity near the surface of the sheet for small value of Darcy number ($Da = 0.01$) as compared to moderate value of Darcy number ($Da = 0.1$).

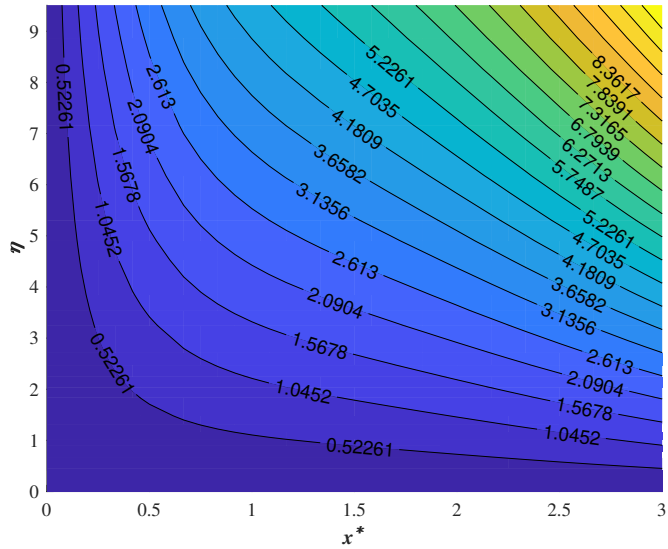

Fig.5.4(a): *Variation of stream lines when* $M^2 = 0$, $C = 1$, $Da = 0.1$, $\lambda = 0.5$

From Figs.5.4(e)-5.4(f), it is found that for couple stress parameter ($C = 5$) behaviour of the stream lines are much thicker as compared to $C = 0$. In Figs.5.4(g)-5.4(h), it is found that stream lines very slightly distort with increasing slip parameter λ. There is a good agreement with the existing literature [312].

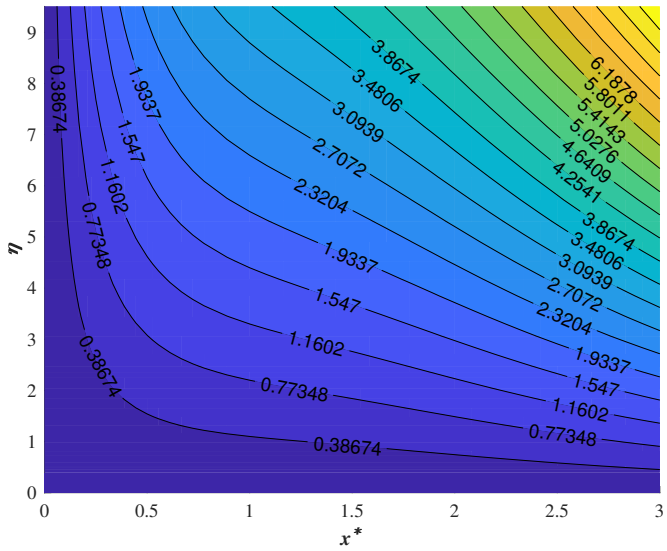

Fig.5.4(b): *Variation of stream lines when* $M^2 = 10$, $C = 1$, $Da = 0.1$, $\lambda = 0.5$

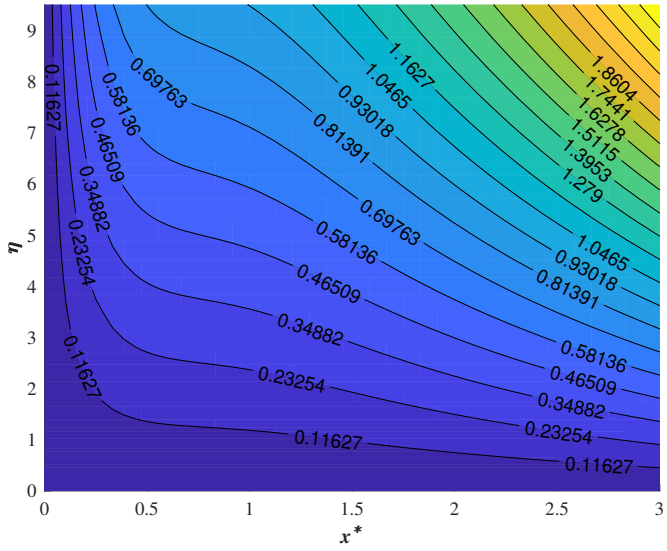

Fig.5.4(c): *Variation of stream lines when* $Da = 0.01$, $C = 1$, $M^2 = 5$, $\lambda = 0.5$

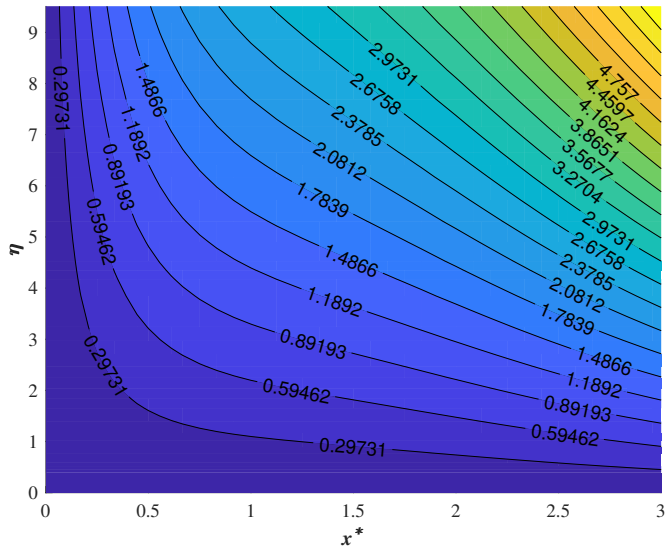

Fig.5.4(d): *Variation of stream lines when* $Da = 0.1$, $C = 1$, $M^2 = 5$, $\lambda = 0.5$

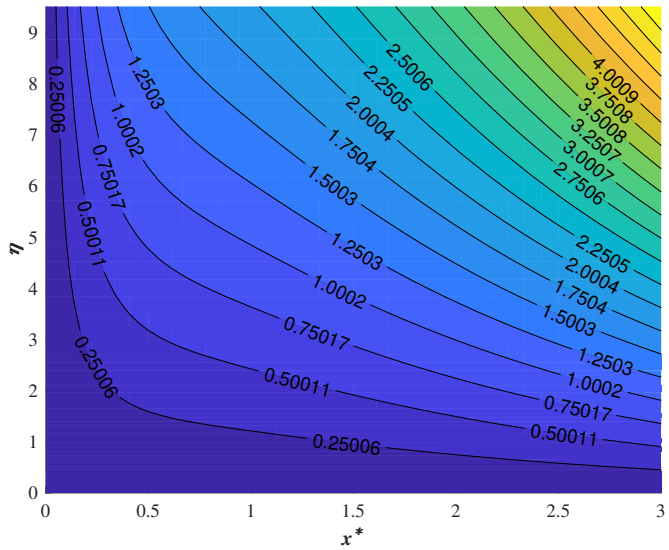

Fig.5.4(e): *Variation of stream lines when* $C = 0$, $M^2 = 5$, $Da = 0.1$, $\lambda = 0.5$

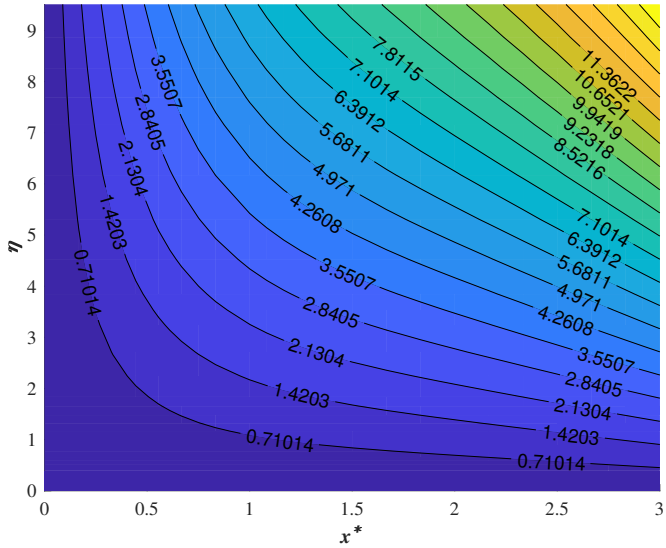

Fig.5.4(f): *Variation of stream lines when* $C = 5$, $M^2 = 5$, $Da = 0.1$, $\lambda = 0.5$

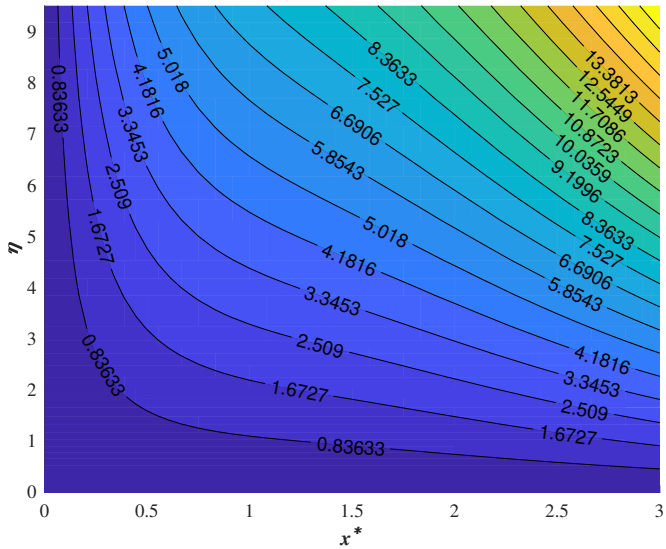

Fig.5.4(g): *Variation of stream lines when* $\lambda = 0$, $M^2 = 5$, $C = 1$, $Da = 0.1$

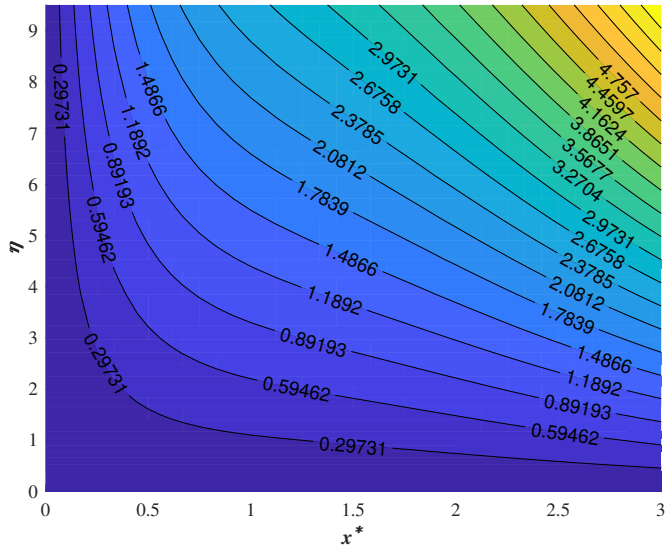

Fig.5.4(h): *Variation of stream lines when* $\lambda = 1$, $M^2 = 5$, $C = 1$, $Da = 0.1$

5.4.4 Effects of parameters on shear stress and rate of heat transfer

For engineering importance, one is usually interested in the values of physical quantities, viz. the shear stress (or skin friction) and the heat transfer rate. The increased shear stress is generally treated as a drawback in engineering applications while the increased heat transfer can be exploited in some applications. Numerical values of the non-dimensional shear stress $-f''(0)$ and the rate of heat transfer $\theta'(0)$ at $\eta = 0$ of the surface of the sheet are recorded in Table 5.2 for several values of physical parameters M^2, C, Da, λ, N, Pr and Ec. The non-dimensional shear stress $-f''(0)$ is found to enhance with increasing M^2 while it reduces with an increase in either C or Da or λ. From physical point of view, it can be noticed that the Lorentz force generates the frictional force and results an increases in shear stress at the sheet surface. Larger values of couple-stress parameter C ($C \to \infty$) contribute less viscous force which reduces frictional force at the sheet surface. The shear stress is reduced with slip parameter λ. This is due to the related fact that when slip phenomenon occurs, the stretching sheet exerts a force that can be transferred to the fluid partially. Increasing value of λ leads to reduce the frictional force at sheet surface. The negative values of shear stress ($-f''(0)$) signify that the sheet surface demonstrates a drag force on the fluid and positive means the opposite.

Table 5.2: *Shear stress $-f''(0)$ and the rate of heat transfer $\theta'(0)$ at the sheet surface ($\eta = 0$)*

M^2	C	Da	λ	N	Pr	Ec	$-f''(0)$	$\theta'(0)$
1	1	0.1	0.5	0.1	7.2	1	0.92429	0.51166
5	1	0.1	0.5	0.1	7.2	1	0.96588	2.93094
10	1	0.1	0.5	0.1	7.2	1	1.00449	5.30325
5	0.5	0.1	0.5	0.1	7.2	1	1.04067	2.59847
5	1	0.1	0.5	0.1	7.2	1	0.96588	2.93094
5	2	0.1	0.5	0.1	7.2	1	0.88846	3.34413
5	1	0.01	0.5	0.1	7.2	1	1.22006	2.29104
5	1	0.1	0.5	0.1	7.2	1	0.96588	2.93094
5	1	0.5	0.5	0.1	7.2	1	0.86431	3.41993
5	1	0.1	0.1	0.1	7.2	1	1.58098	8.83262
5	1	0.1	0.5	0.1	7.2	1	0.96588	2.93094
5	1	0.1	1	0.1	7.2	1	0.65070	0.98953
5	1	0.1	0.5	0.1	7.2	1	0.96588	2.93094
5	1	0.1	0.5	0.5	7.2	1	0.96588	1.44638
5	1	0.1	0.5	1	7.2	1	0.96588	0.54503
5	1	0.1	0.5	0.1	0.71	1	0.96588	0.32274
5	1	0.1	0.5	0.1	1	1	0.96588	0.46298
5	1	0.1	0.5	0.1	7.2	1	0.96588	2.93094
5	1	0.1	0.5	0.1	7.2	0	0.96588	0.61131
5	1	0.1	0.5	0.1	7.2	0.5	0.96588	2.93094
5	1	0.1	0.5	0.1	7.2	1	0.96588	5.25058

In Table 5.2, it is revealed that the rate of heat transfer $\theta'(0)$ increases for increasing values of M^2 or C or Da or Pr or Ec while it decreases for increasing values of N or λ. Due to the influence of thermal radiation, the temperature gradient decreases which eventually reduces the rate of heat transfer at the sheet surface. Therefore, thermal radiation plays an important role in reducing heat transfer rate at sheet surface. Thus, increasing couple stresses imply more intermolecular cohesion which creates more heat hence the fluid temperature as well as the rate of heat transfer are enhanced. The rate of heat transfer $\theta'(0)$ is found to elevate as Eckert number Ec evolves. This may

be aspected that increase in fluid temperature due to viscous heating may decrease fluid viscosity, since viscosity is temperature dependent. The rate of heat transfer is observed to enhance with Prandtl number. This is quite obvious. An increase in Prandtl number reduces the thermal boundary layer thickness. Prandtl number signifies the ratio of momentum diffusivity to thermal diffusivity. Fluids with lower Prandtl number possess higher thermal conductivities (and thicker thermal boundary layer structures), so that heat can diffuse from the sheet surface faster than for higher Pr fluids (thinner boundary layers). Prandtl number has no effective impact on shear stress at the sheet surface as the momentum boundary layer equation is independent of θ. On the other hand, $\theta'(0) > 0$ means the heat transfer take places from fluid to the surface of the sheet.

5.5 Conclusion

The MHD slip flow and heat transfer of an electrically conducting Boussenesq couple-stress fluid over an exponentially stretching sheet embedded in a porous medium subject to the variable magnetic field and thermal radiation has been numerically presented. By means of similarity transformation the governing equations of the modelled problem are converted into non-linear ordinary differential equations which are solved by making the use of shooting iteration technique along with the fourth order Runge-Kutta integration. The main findings of the present analysis are listed below:

- The velocity profile is found to decrease with strengthening of magnetic field.
- The velocity profile boosts with a rise in Darcy number.
- The velocity is observed to reduce when slip parameter is increased.
- The temperature profile is observed to increase with the increase in magnetic parameter or Eckert number while it decreases with an increase in radiation parameter or Darcy number.
- The magnetic parameter is observed to enhance the growth of thermal boundary layer thickness.
- Stream lines distort in the presence of porous materials.
- Both the shear stress and rate of heat transfer at sheet surface are reduced by increasing the slip parameter.

- The shear stress at the surface of the stretching sheet enhances considerably with elevation of magnetic filed.
- Increasing the Prandtl number results in reduction of thermal boundary layer thickness. Consequently, the rate of heat transfer increases with increasing Prandtl number.